

DISCOVERY OF PULSATIONS AND A POSSIBLE SPECTRAL FEATURE IN THE X-RAY EMISSION FROM ROTATING RADIO TRANSIENT J1819–1458

M. A. McLAUGHLIN,^{1,2} N. REA,^{3,4} B. M. GAENSLER,⁴ S. CHATTERJEE,⁴ F. CAMILO,⁵
M. KRAMER,⁶ D. R. LORIMER,^{1,2} A. G. LYNE,⁶ G. L. ISRAEL,⁷ & A. POSSENTI⁸

Draft version July 2, 2021

ABSTRACT

PSR J1819–1458 is a rotating radio transient (RRAT) source with an inferred surface dipole magnetic field strength of 5×10^{13} G and a 4.26-s spin period. We present *XMM-Newton* observations of the X-ray counterpart of this source, CXOU J181939.1–145804, in which we identify pulsations and a possible spectral feature. The X-ray pulsations are at the period predicted by the radio ephemeris, providing an unambiguous identification with the radio source and confirmation of its neutron star nature. The X-ray pulse has a 0.3–5 keV pulsed fraction of 34% and is aligned with the expected phase of the radio pulse. The X-ray spectrum is fit well by an absorbed blackbody with $kT = 0.14$ keV with the addition of an absorption feature at 1 keV, with total absorbed flux of 1.5×10^{-13} ergs cm⁻² s⁻¹ (0.3–5 keV). This absorption feature is well modeled by a Gaussian or resonant cyclotron scattering model, but its significance is dependent on the choice of continuum model. We find no evidence for any X-ray bursts or aperiodic variability on timescales of 6 ms to the duration of the observation and can place the most stringent limit to date of $\leq 3 \times 10^{-9}$ ergs cm⁻² s⁻¹ on the absorbed 0.3–5 keV flux of any bursts.

Subject headings: pulsars: individual (J1819–1458) — radio continuum: stars — stars: flare, neutron — X-rays: stars

1. INTRODUCTION

In 2006 February, a new class of neutron stars, the “Rotating Radio Transients” (RRATs) was reported (McLaughlin et al. 2006). These 11 objects, characterized by repeated dispersed radio bursts, have periods ranging from 0.7 to 7 seconds and are located in the Galactic plane at 2 – 7 kpc distances. Their periods are longer than those of most normal radio pulsars and similar to those of the populations of X-ray dim isolated neutron stars (XDINS; see Haberl 2007 for a review) and magnetars (see Woods & Thompson 2006 for a review). For the three sources with the highest pulse detection rates, period derivatives, \dot{P} , have been determined. If the measured \dot{P} values are interpreted as due to magnetic dipole spin-down, they imply characteristic ages and magnetic field strengths in the general range of the normal pulsar population.

There have been several suggestions put forward on the nature of this new class of neutron star. One obvious suggestion is that the RRATs are related to pulsars which emit “giant pulses” (e.g. Knight et al. 2006). However, the RRATs with measured period derivatives do not appear to have high values of either magnetic field strength at the light cylinder or spin-down luminosity, both suggested as predictors of giant-pulse activity (Cognard et al. 1996; Knight et al. 2006). Zhang et

al. (2006) suggest that the RRATs may be neutron stars near the radio “death line” or may be related to “nulling” radio pulsars. However, the period derivatives measured for three RRATs do not place them near canonical pulsar “death lines” (e.g. Chen & Ruderman 1993) and, unlike most nulling pulsars (e.g. Wang et al. 2007), we typically do not see more than one pulse from the RRATs in succession. Another intriguing possibility is that the sporadicity of the RRATs is due to the presence of a circumstellar asteroid belt (Cordes & Shannon 2006; Li 2006) or a radiation belt such as seen in planetary magnetospheres (Luo & Melrose 2007). Or, perhaps, they are transient X-ray magnetars, a particularly relevant suggestion given the recent detection by Camilo et al. (2006) of transient radio pulsations from the anomalous X-ray pulsar XTE J1810–197. A final possibility is that they are similar objects to PSR B0656+14, one of three middle-aged pulsars (i.e. “The Three Musketeers”; Becker & Truemper 1997) from which pulsed high-energy emission has been detected (e.g. DeLuca et al. 2005). Weltevrede et al. (2006) convincingly show that if PSR B0656+14 were more distant its emission properties would appear similar to those of the RRATs. Determining the reason for the unusual emission of the RRATs is important as population analyses show that their population may be up to several times greater than that of the normal radio pulsars (McLaughlin et al. 2006). Popov et al. (2006) show that the inferred birthrate of RRATs is consistent with that of XDINS but not with magnetars.

While the radio emission properties of J1819–1458 are quite different from those of “normal” pulsars, it appears to be a rotating neutron star from which we detect radio pulses, and we henceforth give it the prefix “PSR”. PSR J1819–1458 shows the brightest and most frequent radio bursts of any of the RRAT sources. It has a 4.26-s period, relatively high inferred characteristic surface dipole magnetic field strength of 5×10^{13} G, characteristic age of 117 kyr, and spin-down luminosity of 3×10^{32} ergs s⁻¹. The distance inferred from its dis-

¹ Department of Physics, West Virginia University, Morgantown, WV 26501.

² National Radio Astronomy Observatory, Green Bank, WV 24944.

³ SRON – Netherlands Institute for Space Research, Sorbonnelaan, 2, 3584 CA, Utrecht, The Netherlands.

⁴ School of Physics, The University of Sydney, NSW 2006, Australia

⁵ Columbia Astrophysics Laboratory, Columbia University, New York, NY 10027.

⁶ Jodrell Bank Observatory, University of Manchester, Macclesfield, Cheshire SK11 9DL, UK.

⁷ INAF – Osservatorio Astronomico di Roma, I-00040 Monteporzio Catone, Italy.

⁸ INAF – Osservatorio Astronomico di Cagliari, Loc. Poggio dei Pini, 09012 Capoterra, Italy.

persion measure (DM) of 196 ± 3 pc cm $^{-3}$ is 3.6 kpc (Cordes & Lazio 2002), with considerable (at least 25%) uncertainty. PSR J1819–1458 is characterized by radio bursts at 1.4 GHz of average duration 3 ms, with bursts arriving randomly with a mean rate of one every ~ 3 minutes. X-ray emission was detected from this source in a serendipitous 30-ks *Chandra* ACIS-I observation toward the Galactic supernova remnant G15.9+0.2 (Reynolds et al. 2006)⁹. They found that the spectrum was well described by an absorbed blackbody with neutral hydrogen column density $N_H = 7_{-4}^{+7} \times 10^{21}$ cm $^{-2}$ and temperature $kT = 0.12 \pm 0.04$ keV, with an absorbed flux of $\sim 1 \times 10^{-13}$ ergs cm $^{-2}$ s $^{-1}$ between 0.3 and 5 keV. These properties are consistent with emission from a cooling neutron star of age $10^4 - 10^5$ years, broadly consistent with the characteristic age of PSR J1819–1458. No evidence for bursts or variability was found. The time resolution of these *Chandra* observations was not sufficient to allow a robust search for X-ray pulsations.

We were awarded 43 ks of *XMM-Newton* time to further characterize the spectrum and search for pulsations. We report here on the results of these observations, in particular the detection of X-ray pulsations and a possible feature in the X-ray spectrum. This is the first detection of X-ray pulsations from any of the RRAT sources. In Section 2 we describe the observations and both the timing and spectral analyses. In Section 3 we discuss possible interpretations of our results, and present our conclusions in Section 4.

2. OBSERVATIONS AND ANALYSIS

The *XMM-Newton* observations were performed on 2006 5 April, with a total observation time of 43 ks. The European Photon Imaging Camera (EPIC) PN and MOS instruments were operated with medium filters and in Small Window mode, providing a time resolution of 6 and 300 ms and effective livetimes of 71% and 97.5%, respectively. The data were reduced using the *XMM-Newton* Science Analysis System (SAS version 7.0.0) and the most recent calibration files. Data from both the PN and MOS instruments were used for the timing and spectral analyses. We also analyzed the Reflection Grating Spectrometer data but our target was too faint to be reliably detected.

We filtered the observation for background flares, resulting in effective on-source exposure times of 32.5 and 37.8 ks (23.0 and 36.9 ks including deadtime) for the PN and MOS instruments, respectively. We detect a point source with J2000 coordinates: right ascension $\alpha = 18^{\text{h}}19^{\text{m}}34^{\text{s}}$ and declination $\delta = -14^{\circ}58'03''$ (4'' error in each coordinate). This is consistent with the radio-timing-derived position and with the more accurate position for the X-ray counterpart published in Reynolds et al. (2006). There is no evidence for extended emission, with the source brightness falling off as expected given the *XMM-Newton* point spread function.

For both PN and MOS data, we extracted the source photons within a 20'' circular radius centered on the source position, which ensured extraction of more than 90% of the source counts. Following standard practice, the size of the extraction region has not been corrected for in our final quoted fluxes and luminosities. The background counts were extracted from four 20'' circular regions centered on off-source positions (different for the PN and MOS instruments) in the same central CCD.

2.1. Timing Analysis

For the timing analysis, we used all photons from PN and MOS1 and MOS2 instruments with PATTERN ≤ 12 (i.e. allowing for single, double, triple and quadruple events¹⁰). This resulted in 2200 ± 58 and 945 ± 15 source and background PN counts and 1380 ± 41 and 230 ± 8 source and background MOS1 plus MOS2 counts (normalized for a 20'' circular extraction region). Although we can measure a period of 4.26 s from the arrival times of the radio bursts, the periodicity is not detectable in a Fast Fourier Transform of the radio time series due to the sporadic nature of the source. We therefore performed a periodicity search of all PN and MOS photons (i.e. with energies 0.2–15 keV) as a confirmation of the method through which the radio period was derived (see McLaughlin et al. 2006). The arrival times were converted to the solar system barycenter and the Z_1^2 test (Buccheri et al. 1983) was applied. The most significant signal is detected with $Z_1^2 = 144.5$ at a frequency of 234.564 ± 0.007 mHz (all errors are quoted at the 1σ confidence level). Allowing for 4.3×10^6 independent frequencies searched in the range 0.1–100 Hz, the probability of chance occurrence of this signal in the absence of a real pulsation would be 1.8×10^{-25} , showing that the periodicity from this source would be easily detectable in a blind search of the X-ray photons.

The ephemeris obtained through continued radio timing of PSR J1819–1458 with the Parkes radio telescope at 1.4 GHz using the TEMPO software package predicts a barycentric frequency at the center of the observation (MJD 53830.87029) of 234.566244 ± 0.000001 mHz, consistent with the measured X-ray frequency. Accounting for spin-down during the observation is unimportant as the change in frequency due to the -3.16×10^{-14} Hz s $^{-1}$ frequency derivative over the 12-hr observation is much less than the size of an individual frequency bin. The X-ray detection of periodicity shows that the radio-derived period is indeed the true period, and not a smaller common factor of the radio arrival times (see McLaughlin et al. 2006).

In Figure 1, we present the 0.3–5 keV background-corrected X-ray pulse profile formed by folding barycentered photons from the PN and both MOS instruments using the radio ephemeris. The same good time interval file was used for the PN and both MOS instruments and backgrounds were subtracted separately. The different exposure times for the two instruments were accounted for. We chose to restrict this analysis to 0.3–5 keV as below 0.3 keV, the PN and MOS detectors are not well calibrated and, above 5 keV, the background dominates. In Figure 1, we also present the radio profile formed from adding individual bright radio pulses with the radio ephemeris. The X-ray pulse profile has a 0.3–5 keV background-corrected pulsed fraction of $34 \pm 6\%$, defined as $(F_{\text{max}} - F_{\text{min}})/(F_{\text{max}} + F_{\text{min}})$, where F_{max} and F_{min} are the minimum and maximum values of the X-ray pulse profile. It can be well modeled as a single sinusoid with $\chi^2_{\nu} \sim 1.2$ (17 d.o.f.). We find no significant dependence of pulsed fraction on energy, with a pulsed fraction at energies 0.3–1 keV of $28 \pm 7\%$ and a pulsed fraction at energies from 1–5 keV of $49 \pm 10\%$.

The peak of the X-ray profile, calculated by fitting a sinusoid, is at phase 0.49 ± 0.04 and is aligned to the peak of the radio profile at phase 0.5. The 3 pc cm $^{-3}$ uncertainty in the DM of 196 pc cm $^{-3}$ amounts to a radio arrival time uncer-

⁹ As discussed by Reynolds et al. (2006), an association between the remnant and PSR J1819–1458 is extremely unlikely.

¹⁰ http://xmm.vilspa.esa.es/external/xmm_user_support/documentation/uhb

tainty at 1.4 GHz of only 13 ms, or 0.3% of the 4.26 s pulse period.

Our PN data can be used to place limits on the existence of X-ray bursts from the source. Binning the data on various timescales to search for bursts of different widths we find no evidence for aperiodic variability on timescales ranging from 6 ms to the duration of our observation. We used photons with energies up to 10 keV, important given the hard spectra of magnetar bursts (e.g. Gavriil et al 2004). Omitting frames with high particle background, we find that none of the 4×10^6 frames contains more than two counts within the $20''$ region, with three frames containing exactly two counts. These numbers are entirely consistent with Poisson statistics. The number of events in a single frame which would deviate from a steady flux at the $3\text{-}\sigma$ level is 3 photons. We therefore adopt this as the upper limit on the X-ray flux of any burst of width 6 ms or less. Assuming a spectrum of the same shape as that fitted for the overall source (column 2 of Table 1; see Section 2.2) limits the observed fluence of any burst to $\lesssim 8 \times 10^{-12}$ ergs cm^{-2} (0.3–5 keV), corresponding to an absorbed flux limit of $\lesssim 3 \times 10^{-9}$ ergs $\text{cm}^{-2} \text{ s}^{-1}$ (0.3–5 keV) if we assume that the X-ray burst would last for 3 ms, the width of the radio pulse. This is a factor of five better than the limits placed by Reynolds et al. (2006). At a distance of 3.6 kpc, these limits correspond to a total energy of 2×10^{34} ergs and luminosity of 1×10^{37} ergs s^{-1} . Therefore, any bursts, at least during the 12-hour duration of our observation, must contain much less energy than typical X-ray magnetar bursts (e.g. Woods & Thompson 2006) if their spectra is indeed similar to that described in column 2 of Table 1.

2.2. Spectral Analysis

For the spectral analysis, we used PN photons with $\text{PATTERN} \leq 4$ (i.e. single and double events) and MOS1 and MOS2 photons with $\text{PATTERN} \leq 12$. Source and background spectra were extracted from the same regions used for the timing analysis and the spectral response matrices were created with the SAS `mkrmf` and `mkarf` tools, using the bad-pixel file built for our observation. The PN and MOS spectra were only used in the 0.4–2 keV energy range, a smaller range than that used for the timing analysis due to the greater dependence of spectral fitting on background spectra. In the spectral analysis we used both rebinned and unbinned spectra. Spectra were rebinned for MOS and PN by a factor of two so that the energy resolution was not oversampled by more than a factor of three (using the specific response matrix built for this observation). Furthermore, we rebinned in order to have at least 30 counts per bin so that we could use the χ^2 statistic¹¹.

We first modeled the PN spectrum. We tried several different models and found that a single component fit was not possible. Fitting with a single absorbed¹² blackbody (as in Reynolds et al. 2006), we found $N_H \sim 4.0 \times 10^{21} \text{ cm}^{-2}$ and $kT \sim 0.14 \text{ keV}$ with a $\chi^2_\nu > 2.0$ (see Figure 2), while for an absorbed powerlaw, we obtained $N_H \sim 1.3 \times 10^{22} \text{ cm}^{-2}$ and $\Gamma \sim 8.2$ with a $\chi^2_\nu > 2.1$ (both fits have 53 d.o.f). These values are consistent with the Reynolds et al. (2006) best-fit parameters (0.5–8 keV) of $N_H = 7^{+7}_{-4} \times 10^{21} \text{ cm}^{-2}$ and $kT = 0.12 \pm 0.04 \text{ keV}$ (for the absorbed blackbody model) and $\Gamma \sim 9.5$ (for the power-law model). An inspection of the resid-

uals revealed that our high χ^2_ν values were due to the presence of strong spectral features around 1 keV and a weaker one around 0.5 keV.

We carefully checked whether these features might be due to calibration issues, to our source and background extraction regions or to residual particle flares and/or particles hitting the detector. We reliably excluded all of these issues by studying in detail the *XMM-Newton* calibration lines (see Figure 3), extracting the source and background photons from several different regions and investigating the spectrum using only $\text{PATTERN} = 0$ counts (i.e. only isolated events). However, we note that the 0.5 keV feature is very close to the Oxygen edge energy, and an overabundance of Oxygen in the direction of the source could be responsible. To further investigate this possibility, we fit our spectrum with an absorbed blackbody model using three different photoelectric cross-sections, those of Bałucińska-Church & McCammon (1992, 1998) and of Verner et. al. (1996). This was aimed at studying the dependence of the significance of our 0.5 keV line on the chosen photoelectric cross-section, which drives the shape of the edge. We found that the residuals around 0.5 keV remain in all cases, although less significantly if we use the Verner et. al. (1996) cross-section. For that reason, we assumed this cross-section for all our spectral fitting, and we omitted all photons in the 0.50–0.53 keV energy range (two bins in our rebinned PN spectrum) from our modeling. We tentatively conclude that this line is due to the Oxygen edge, but only future deeper observations will unambiguously confirm this.

Keeping the number of components as low as possible, we tried to model our rebinned PN spectrum with either an absorbed blackbody (XSPEC model `bbbody`) or power-law (`powerlaw`), in addition to modeling the $\sim 1 \text{ keV}$ feature in several ways: leaving free the abundances of the most abundant elements in the interstellar medium (ISM) with lines around 1 keV (e.g. Ne, N, Mg, Fe), adding a Gaussian function (XSPEC model `gabs`), a Lorentzian function (`lorentz`), an absorption edge (`edge`) or a cyclotron resonant scattering model (`cyclabs`). Among our trials, only the models reported in Table 1 gave satisfactory values of $\chi^2_\nu \sim 1$. We show the blackbody plus Gaussian fit and residuals in Figure 4. Note that there is evidence in the residuals for narrow lines within our broad 1 keV line, implying that the line may be a blending of narrower lines. However, the addition of several single narrow lines is not statistically significant, and future data with better statistics are necessary for investigating this issue.

We ran Monte Carlo simulations of 2×10^4 spectra (see Rea et al. (2005, 2007) for details) to estimate the significance of the spectral feature (as suggested by Protassov et al. 2002)¹³. The spectra were simulated using models corresponding to columns 2 and 4 from Table 1 with the absorbed blackbody parameters varying within their 3σ errors (see Table 1), absorption line parameters completely free to vary, and fixing the number of counts of each spectra at the PN count value for PSR J1819–1458. After having generated 10^4 spectra for each of the two models, we counted how many of these simulated spectra showed an absorption feature at any energy, width or depth, only due to statistical fluctuations. None of the simulated spectra presented a Gaussian absorption line at any energy or width with a depth $\tau_G > 30$, and no cyclotron

¹¹ <http://heasarc.nasa.gov/xanadu/xspec/manual/manual.html>

¹² If not otherwise specified, abundances were assumed to be solar and fixed at the values in Lodders (2003).

¹³ Even though the F-test is still widely used to assess the significance of features in X-ray spectra, it has been shown that this is not statistically correct (Protassov et al. 2002).

TABLE 1
SPECTRAL FITS FOR PSR J1819–1458 WITH EPIC-PN

	Blackbody (BB) plus Neon	BB plus Gaussian	BB plus edge	BB plus cyclotron
N_H	$0.59^{+0.06}_{-0.04}$		$0.75^{+0.12}_{-0.09}$	0.57 ± 0.06
N_{Ne}	6 ± 1	E_G	$1.11^{+0.04}_{-0.03}$	E_e
		σ_G	$0.21^{+0.03}_{-0.06}$	E_{cy}
		τ_G	150 ± 60	w_{cy}
			τ_e	d_{cy}
kT	$0.144^{+0.008}_{-0.006}$	$0.136^{+0.012}_{-0.008}$	$0.150^{+0.005}_{-0.006}$	$0.144^{+0.008}_{-0.006}$
Abs. Flux	$1.5^{+0.3}_{-0.5}$	$1.5^{+0.6}_{-0.8}$	$1.5^{+0.3}_{-0.6}$	$1.5^{+0.3}_{-0.4}$
Unab. Flux	15 ± 2	26^{+2}_{-8}	12^{+2}_{-2}	34^{+4}_{-9}
χ^2_ν (d.o.f.)	1.20 (50)	1.19 (48)	1.17 (49)	1.13 (48)

NOTE. — Fluxes are calculated in the 0.3–5 keV energy range, and reported in units of 10^{-13} ergs s^{-1} cm^{-2} . N_H is in units of 10^{22} cm^{-2} and N_{Ne} is in solar units (always assuming solar abundances from Lodders 2003). The photoelectric cross-section of Verner et al. (1998) has been used for all fits. The values of kT (blackbody temperature), E_G (Gaussian line energy), σ_G (Gaussian line width), E_e (edge threshold energy), E_{cy} (cyclotron line energy) and w_{cy} (cyclotron line width) are in units of keV. The Gaussian line depth τ_G , edge depth τ_e and fundamental cyclotron line depth d_{cy} are dimensionless. Errors are at the 1σ confidence level. XSPEC models used are (from left to right): `vphabs*bbbody`, `phabs*gabs*bbbody`, `phabs*edge*bbbody` and `phabs*cyclabs*bbbody`.

component was detected with a depth > 0.3 for any energy or width. We therefore infer the significance of the line at 1 keV to be $> 1/10^4$, corresponding to a $> 99.99\%$ probability (i.e. at least 4σ) that this line is not due to statistical fluctuations.

To check whether the line was also present in the MOS data, we simultaneously fit the PN and both MOS1 and MOS2 rebinned spectra (see Figure 5). All models in Table 1 fit the PN, MOS1 and MOS2 data well. However, because of the lower number of MOS counts, our 1 keV line was not significant in the MOS spectra, especially because the rebinning we did in order to use the χ^2 statistic left only a handful of bins within the line. As a further check, we then used the unbinned PN and MOS spectra and the C-statistic (Cash 1979) to assess the goodness of an absorbed blackbody fit, without the inclusion of any line. We found that for $N_H = 0.5 \times 10^{22}$ cm^{-2} and $kT = 0.14$ keV, the C-statistic is 1009.776 using 969 PHA bins. A Monte Carlo simulation of the fit showed that the probability of having a C-statistic < 1010 is 98.0%. Note that only if the C-statistic probability is smaller than 50% can the model be accepted. This shows that an absorbed blackbody model alone can not reproduce the data, and hence that a line is also present in the MOS spectra. We show in Figure 5 the PN, MOS1 and MOS2 spectra modeled with an absorbed blackbody plus a Gaussian (column 2 in Table 1), with a more severe PN rebinning (with at least 40 counts per bin), to show the agreement between the three instruments. Note that all the models in Table 1 satisfactorily fit the previous *Chandra* data (Reynolds et al. 2006), although the absorption line is not statistically significant in those data because of the reduced number of counts.

Furthermore, we checked whether the spectral feature parameters and significance were dependent on the spectral binning or on the continuum model. We found that the spectral feature does not vary significantly when we vary the amount of spectral binning (see also Figure 5), but that it is rather dependent on the chosen continuum (as is generally the case for every spectral feature). In fact, if instead of a blackbody model, we assume a power-law continuum, the feature is still detectable with similar spectral properties but at a lower significance of 98.9% (roughly 2.5σ).

Hence, if we assume a blackbody continuum model (reasonable for an isolated neutron star) we can show with high

confidence that a spectral feature is present in our data. However, our statistics do not allow us to statistically prefer one model to the others and reliably ascertain its nature. Furthermore, if future, more sensitive observations reveal a different source continuum, the significance of the feature may need to be revised.

We also performed phase-resolved spectroscopy over two intervals of 0.5 in phase centered on the peak and the minimum of the pulse profile, respectively. We did not find any significant spectral variability between these two phase intervals at the 2σ level. However the low number of counts in each spectrum does not allow us to reach any reliable conclusions about the pulse-phase dependence of the spectral parameters.

3. DISCUSSION

3.1. Interpretation of the spectral feature

If we accept that the spectral feature is significant, the two main possible interpretations are as an atomic line or as a cyclotron resonant scattering line.

If the line is atomic, then it could be due either to the neutron star atmosphere or, but less probably, to a peculiar abundances in the ISM in that direction (or perhaps even a combination of the two). At 1 keV, it might then be due to the Ne edge (although improbable given its low abundance), Ne XI K-edge (at 1.19 keV), or some Fe-L lines, including Fe XX, Fe XXI and Fe XXII or Fe XXIII (all around 0.9 keV). Note that Fe lines are common in other kinds of neutron stars, though mostly coming from accretion disks in binary systems rather than from the neutron stars themselves (see e.g. Cottam et al. 2002). The structure present in the residuals (see Figure 4 middle panel), which in our data is not significant, might be due to a blending of narrow lines which we could only model with a broad line due to our limited number of counts.

If the feature is due to proton cyclotron resonant scattering, the magnetic field inferred would be $B_{cy} = 1.6E_{cy}(\text{keV})/y_G 10^{14}$ G, where $y_G = (1 - 2GM/c^2R)^{1/2}$ is the gravitational redshift factor (M and R are the neutron star mass and radius, respectively). Assuming canonical values for M and R of $1.4 M_\odot$ and 10 km, we find $B_{cy} = 2 \times 10^{14}$ G. This is slightly higher than the dipolar surface magnetic field

inferred through radio timing through the standard formula $B = 3.2 \times 10^{19} P \dot{P}^{1/2} = 5 \times 10^{13}$ G. However, this expression can be considered an order-of-magnitude estimate as it assumes a purely dipolar field, a neutron star radius of 10 km, a moment of inertia of 10^{45} g cm² and an angle between the spin and magnetic axes $\alpha = 90$ degrees. Accounting for this and assuming $\alpha = 30$ degrees would make the timing- and cyclotron-inferred fields consistent. In addition, the width and depth of the line are consistent with the predictions of Zane et al. (2001) for proton-cyclotron absorption in highly magnetized neutron stars. We cannot detect any harmonics to the fundamental cyclotron line because our spectrum is background dominated above 2 keV. However, as observed in some accreting sources (Heindl et al. 2004) and investigated for isolated neutron stars by Liu et al. (2006), in some cases the first harmonic is as deep as the fundamental cyclotron frequency. Therefore, it is possible, although unlikely, that the 1 keV feature is the first harmonic, with the 0.5 keV fundamental coincident with the depression in the spectrum that we have interpreted as due to an overabundance of Oxygen. We note that the observed lines are unlikely to be due to electron-cyclotron absorption as the inferred magnetic field would be a factor of 2000 lower (i.e. the ratio of the proton to electron mass) and incompatible with that measured through radio timing.

3.2. Relationship to other classes of neutron stars

Our detection of periodicity at the radio period shows that the X-ray source reported by Reynolds et al. (2006) is undoubtedly the counterpart to PSR J1819–1458. The pulsed fraction and sinusoidal pulse shape are similar to what is observed for other middle-aged X-ray-detected radio pulsars such as B0656+14 (e.g. De Luca et al. 2005), which has been observed to have similar radio properties to the RRATs (Weltevrede et al. 2006).

The thermal emission from PSR J1819–1458 is consistent with a cooling neutron star. However, the temperature from our blackbody fit appears slightly higher than temperatures derived from blackbody fits for other neutron stars of similar ages (see discussion by Reynolds et al. 2006). Note that it is possible that PSR J1819–1458 was born spinning at a sizable fraction of its present period of 4.26 s. In this case, as discussed by Reynolds et al. (2006), the characteristic age could be a considerable overestimate and the inferred temperature could be completely consistent with its age. Note that characteristic ages have been shown to be misleading for several other pulsars (e.g. Gaensler & Frail 2000; Kramer et al. 2003).

Including PSR J1819–1458, eight high-magnetic field radio pulsars (i.e. $B > 1 \times 10^{13}$ G) have now been observed at X-ray energies. Two, J1846–0258 and B1509–58, are bright non-thermal sources (Mereghetti et al. 2002; Cusumano et al. 2001), as expected given their young ages (less than 2000 yr). PSR J1119–6127 is a bright thermal X-ray emitter with unusual properties including a large pulsed fraction and narrow pulse (Gonzalez et al. 2005). PSR J1718–3718, with magnetic field of 7×10^{13} G, has been detected at X-ray energies, but the faintness of the counterpart does not allow detailed spectral modeling or a constraining limit on pulsed fraction (Kaspi & McLaughlin 2005). No X-ray emission has been detected from PSRs J1814–1744, B0154+61 or J1847–0130, which has the highest inferred surface dipole magnetic field (9×10^{13} G) measured to date for any radio pulsar (Pivovarov et al. 2000; Gonzalez et al. 2004; McLaughlin et al. 2003). Radio pulsar X-ray emission properties clearly vary widely,

even for objects with very similar spin-down properties.

While the spectrum and luminosity of PSR J1819–1458 argue against a relationship with magnetars, it is possible that PSR J1819–1458 could be a transition object between the pulsar and magnetar source classes. The soft X-ray spectrum does have a comparable temperature to the quiescent state of XTE J1810–197 ($kT \sim 0.15 - 0.18$ keV; Ibrahim et al. 2004; Gotthelf et al. 2004). However, the radio emission characteristics of these two neutron stars are quite different.

While resonant cyclotron features are regularly observed from X-ray binary systems (e.g. Truemper et al. 1978; Nakajima et al. 2006), the detection of such features from isolated neutron stars is quite unusual. Sanwal et al. (2002) & Mereghetti et al. (2002) discovered harmonically spaced absorption lines from 1E 1207.4–5209, a radio-quiet X-ray pulsar with a 424-ms spin period and timing-derived characteristic age and inferred surface dipole magnetic field strength of 3×10^5 yr and 3×10^{12} G, respectively. Analyzing a deeper observation of the source, Bignami et al. (2003) attributed these lines to electron-cyclotron absorption. However, the significance of two of the lines present in its spectrum has been strongly questioned (Mori et al. 2005).

Broad absorption lines, similar to those seen for PSR J1819–1458, have been observed for six out of seven XDINS (see reviews by van Kerkwijk & Kaplan 2007 and Haberl 2007). For most of these neutron stars, the lines can be interpreted as due to neutral hydrogen transitions in highly magnetized atmospheres. Ho et al. (2003) and Van Kerkwijk & Kaplan (2007) argue that the transition energy is similar to the proton cyclotron energy for magnetic fields of the order of PSR J1819–1458's. The X-ray spectrum of PSR J1819–1458 is very similar (although with a slightly hotter blackbody temperature) to the XDINSs, although so far no convincing evidence for radio bursts has been detected for any of those thermally emitting neutron stars (Kondratiev et al., in preparation).

One outstanding question is why absorption lines of this kind, whether due to the atmosphere or to cyclotron resonant scattering, have been observed from only a handful of X-ray emitting isolated neutron stars. As suggested by Mereghetti et al. (2002), the age of the neutron star could be one key factor. Young objects are dominated by non-thermal emission, but older ones may be too faint for X-rays to be detectable, making X-ray bright, middle-aged pulsars the best candidates (as is the case of the XDINSs and of PSR 1819–1458). Note, however, that no such absorption lines have been found for the X-ray bright, middle-aged PSR B0656+14, despite deep searches both with *Chandra* (Marshall & Schultz 2002) and *XMM-Newton* (De Luca et al. 2005) and the theoretical predictions for cyclotron and/or atmospheric features expected in its emission. The explanation could well depend on the viewing geometry.

More sensitive observations are necessary to confirm the presence of absorption features in the spectrum of PSR J1819–1458. Longer X-ray observations are needed to understand whether the broad 1 keV line could be a blending of narrower features. This would then argue for an atomic origin for the line. Longer observations will also allow phase-resolved spectroscopy. Simulations show that a 100-ks observation would allow us to achieve both of these goals. Because the strength of the cyclotron line depends on the angle between the observer and the magnetic field, we expect phase variation of cyclotron features. If the feature we detect is in-

deed due to proton-cyclotron absorption, it provides an invaluable means of testing the assumptions implicit in the characteristic magnetic fields derived through radio timing measurements and a unique independent measurement of the magnetic field of an isolated neutron star.

4. CONCLUSIONS

We have discovered X-ray pulsations at the 4.26-s period inferred from radio timing of PSR J1819–1458. The properties of these pulsations are similar to those observed for other middle-aged radio pulsars detected at X-ray energies. While the RRATs are characterized by sporadic radio emission, we do not detect any X-ray bursts or aperiodic variations throughout the observation and can place the most stringent limit to date of $\leq 3 \times 10^{-9}$ ergs cm⁻² s⁻¹ on the absorbed 0.3–5 keV flux of any X-ray bursts. We have characterized the spectrum of this source and find that it is well-described by an absorbed blackbody with $kT = 0.14$ keV in addition to

an absorption line around 1 keV, with total absorbed flux of 1.5×10^{-13} ergs cm⁻² s⁻¹ (0.3–5 keV). We note, however, that the presence of this absorption feature is highly dependent on the choice of continuum model and needs further X-ray observations to be confirmed. This object is the only RRAT so far to be detected at X-ray energies. X-ray observations of the other objects in this source class are essential for a complete picture of how they relate to other neutron star populations.

MAM thanks the Parkes Multibeam Survey team for radio observing assistance and Pete Woods for helpful discussions on XMM data analysis. This work was supported by NASA through *XMM-Newton* Observer Program grant NNX06AG20G. N.R. is supported by an NWO Postdoctoral Fellowship and a Short Term Visiting Fellowship awarded by the University of Sydney, and kindly thanks M. Méndez for useful suggestions.

REFERENCES

- Balucińska-Church, M., & McCammon, D. 1992, *ApJ*, 400, 699
 Balucińska-Church, M., & McCammon, D. 1998, *ApJ*, 496, 1044
 Becker, W. & Truemper, J. 1997, *A&A*, 326, 682
 Bhat, N. D. R., Gupta, Y., Kramer, M., Karastergiou, A., Lyne, A. G., & Johnston, S. 2007, *A&A*, 462, 257
 Bignami, G. F., Caraveo, P. A., De Luca, A., & Mereghetti, S. 2003, *Nature*, 423, 725
 Bucccheri, R., et al. 1983, *A&A*, 128, 245
 Camilo, F., Ransom, S. M., Halpern, J. P., Reynolds, J., Helfand, D. J., Zimmerman, N., & Sarkissian, J. 2006, *Nature*, 442, 892
 Cash, W. 1979, *ApJ*, 228, 939
 Chen, K., & Ruderman, M. 1993, *ApJ*, 402, 264
 Cognard, I., Shrauner, J. A., Taylor, J. H., & Thorsett, S. E. 1996, *ApJ*, 457, L81
 Cordes, J. M., & Lazio, T. 2002, astro-ph/0207156
 Cordes, J. M., & Shannon, R. M. 2006, submitted, astro-ph/0605145
 Cottam, J., Paerels, F., & Mendez, M. 2002, *Nature*, 420, 51
 Cusumano, G., Mineo, T., Massaro, E., Nicastro, L., Trussoni, E., Massaglia, S., Hermsen, W., & Kuiper, L. 2001, *A&A*, 375, 397
 De Luca, A., Caraveo, P. A., Mereghetti, S., Negroni, M., & Bignami, G. F. 2005, *ApJ*, 623, 1051
 Gaensler, B. M., & Frail, D. A. 2000, *Nature*, 406, 158
 Gavriil, F. P., Kaspi, V. M., & Woods, P. M. 2004, *ApJ*, 607, 959
 Gonzalez, M. E., Kaspi, V. M., Camilo, F., Gaensler, B. M., & Pivovarov, M. J. 2005, *ApJ*, 630, 489
 Gonzalez, M. E., Kaspi, V. M., Lyne, A. G., & Pivovarov, M. J. 2004, *ApJ*, 610, L37
 Gotthelf, E. V., Halpern, J. P., Buxton, M., & Bailyn, C. 2004, *ApJ*, 605, 368
 Haberl, F. 2007, *Ap&SS*, 308, 73
 Haberl, F., Sembay, S., Altieri, B. & Brinkmann, W. 2006, *ESASP*, 604, 353
 Haberl, F., Zavlin, V. E., Trümper, J., & Burwitz, V. 2004, *A&A*, 419, 1077
 Heindl, W. A. et al., 2004, Proceedings of "X-Ray Timing 2003: Rossi and Beyond", eds. P. Kaaret, F.K. Lamb, & J.H. Swank (Melville, NY: AIP)
 Ho, W. C. G., Lai, D., Potekhin, A. Y., & Chabrier, G. 2003, *ApJ*, 599, 1293
 Ibrahim, A. I., et al. 2004, *ApJ*, 609, L21
 Kaspi, V. M., & McLaughlin, M. A. 2005, *ApJ*, 618, L41
 Knight, H. S. 2006, *Chinese Journal of Astronomy and Astrophysics Supplement*, 6, 41
 Kramer, M., Lyne, A. G., Hobbs, G., Lohmer, O., Carr, P., Jordan, C. & Wolszczan, A. 2003, *ApJ*, 593, L31
 Li, X.-D. 2006, *ApJ*, 646, L139
 Liu, D. B. et al. 2006, *ApJ*, 644, 439
 Lodders, K. 2003, *ApJ*, 591, 1220
 Luo, Q. & Melrose, D. B. 2007, *MNRAS*, 0704.2906
 McLaughlin, M. A., et al. 2003, *ApJ*, 591, L135
 McLaughlin, M. A., et al. 2006, *Nature*, 439, 817
 Mereghetti, S., Bandiera, R., Bocchino, F., & Israel, G. L. 2002, *ApJ*, 574, 873
 Mereghetti, S., De Luca, A., Caraveo, P. A., Becker, W., Mignani, R., & Bignami, G. F. 2002, *ApJ*, 581, 1280
 Mori, K., Chonko, J. C., & Hailey, C. J. 2005, *ApJ*, 631, 1082
 Nakajima, M., Mihara, T., Makishima, K., & Niko, H. 2006, *ApJ*, 646, 1125
 Pivovarov, M. J., Kaspi, V. M., & Camilo, F. 2000, *ApJ*, 535, 379
 Popov, S. B., Turolla, R., & Possenti, A. 2006, *MNRAS*, 369, L23
 Protassov, R., van Dyk, D. A., Connors, A., Kashyap, V. L., & Siemiginowska, A. 2002, *ApJ*, 571, 545
 Rea, N., et al. 2005, *MNRAS*, 361, 710
 Rea, N., et al. 2007, *Ap&SS*, 308, 505
 Reynolds, S. P. et al. 2006, *ApJ*, 639, L71
 Sanwal, D., Pavlov, G. G., Zavlin, V. E., & Teter, M. A. 2002, *ApJ*, 574, L61
 Schwobe, A. D., Hambaryan, V., Haberl, F., & Motch, C. 2007, *Ap&SS*, 106
 Truemper, J., Pietsch, W., Reppin, C., Voges, W., Staubert, R., & Kendziorra, E. 1978, *ApJ*, 219, L105
 van Kerkwijk, M. H., & Kaplan, D. L. 2007, *Ap&SS*, 308, 74
 Verner, D. A., Ferland, G. J., Korista, K. T., & Yakovlev, D. G. 1996, *ApJ*, 465, 487
 Wang, N., Manchester, R. N., & Johnston, S. 2007, *MNRAS*, 377, 1383
 Weltevrede, P., Stappers, B. W., Rankin, J. M., & Wright, G. A. E. 2006, *ApJ*, 645, L149
 Woods, P. M., et al. 2005, *ApJ*, 629, 985
 Woods, P. M. & Thompson, C. 2006, "Compact Stellar X-ray Sources", eds. W. H. G. Lewin & M. van der Klis, 547
 Zane, S., Turolla, R., Stella, L., & Treves, A. 2001, *ApJ*, 560, 384
 Zhang, B., Gil, J., & Dyks, J. 2007, *MNRAS*, 374, 1103

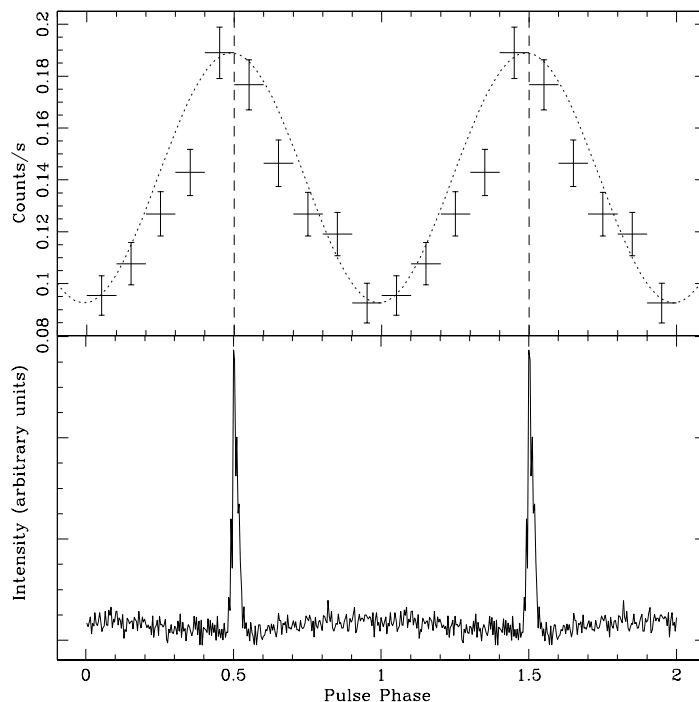


FIG. 1.— Top: X-ray pulse profile (0.3–5 keV) for 23-ks of EPIC-PN data and 37-ks of MOS1 and MOS2 data on PSR J1819–1458. The dotted line shows the best-fit sinusoid and the vertical dashed line indicates the phase of the peak of the radio pulse. Bottom: radio profile formed from 114 pulses detected in 6 hr of observation at 1.4 GHz with the Parkes telescope in Australia. The non-uniform baseline is likely due to instrumental digitization effects. Both profiles have been folded using the radio ephemeris. In both plots, two cycles of pulse phase are shown.

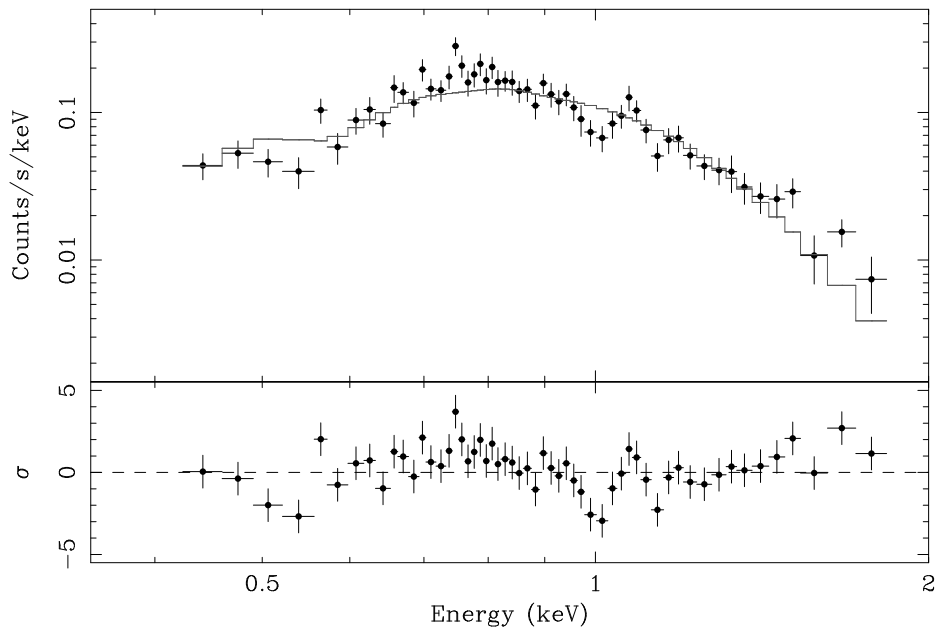


FIG. 2.— Top: *XMM-Newton* EPIC-PN spectrum of PSR J1819–1458, modeled as an absorbed blackbody. The points indicate the data, while the solid line shows the corresponding best-fit model. Bottom: residuals of the model.

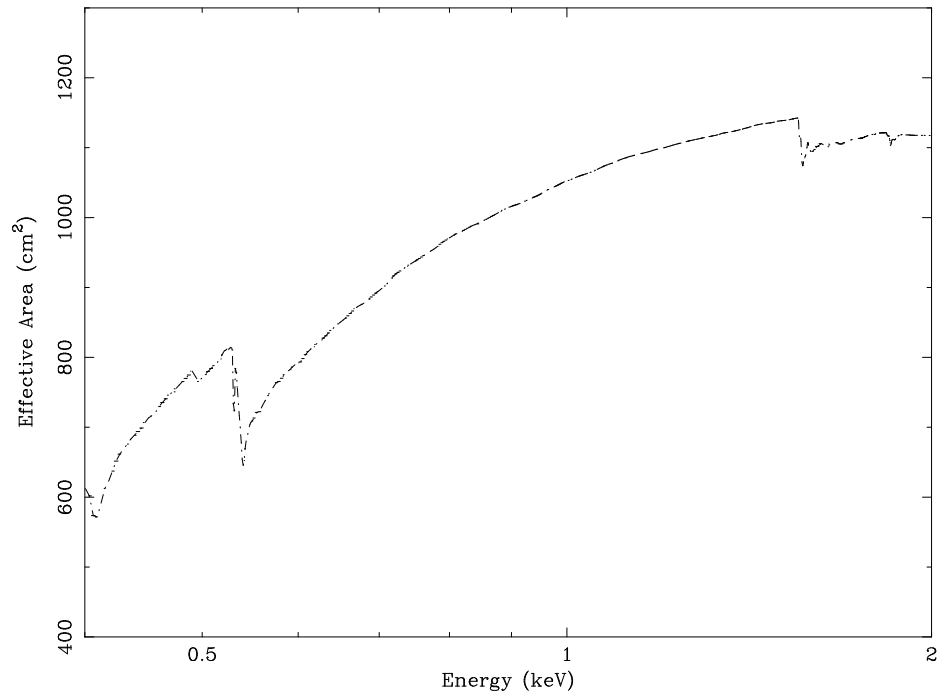


FIG. 3.— The effective area, or total response efficiency, for EPIC-PN with the medium filter versus incident photon energy. Note that there is no instrumental feature in the effective area curve at 1 keV. The calibration feature near 0.5 keV is too weak to explain the feature in our spectrum close to this energy (see Haberl et al. 2006 for more details on *XMM-Newton* calibration.)

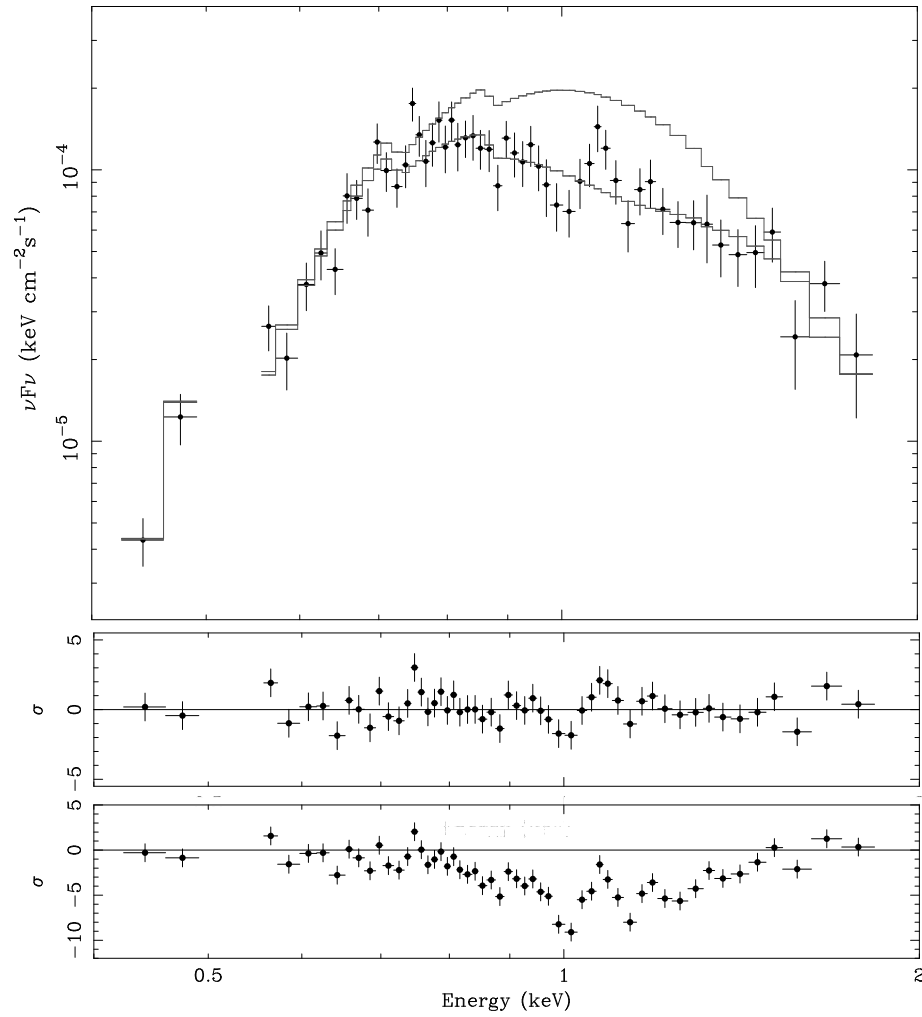


FIG. 4.— Top: *XMM-Newton* EPIC-PN νF_ν spectrum of PSR J1819–1458, modeled as an absorbed blackbody and Gaussian line (column 2 of Table 1). The points indicate the data, while the solid line shows the corresponding best fit model. Top line shows the absorbed blackbody model component of the fit alone. We have omitted all photons with energies from 0.5–0.53 keV as we believe that the feature in this range is due to the Oxygen edge (see Section 2.2). Middle: residuals of the absorbed blackbody and Gaussian line model. Bottom: residuals of the model without the inclusion of the Gaussian line.

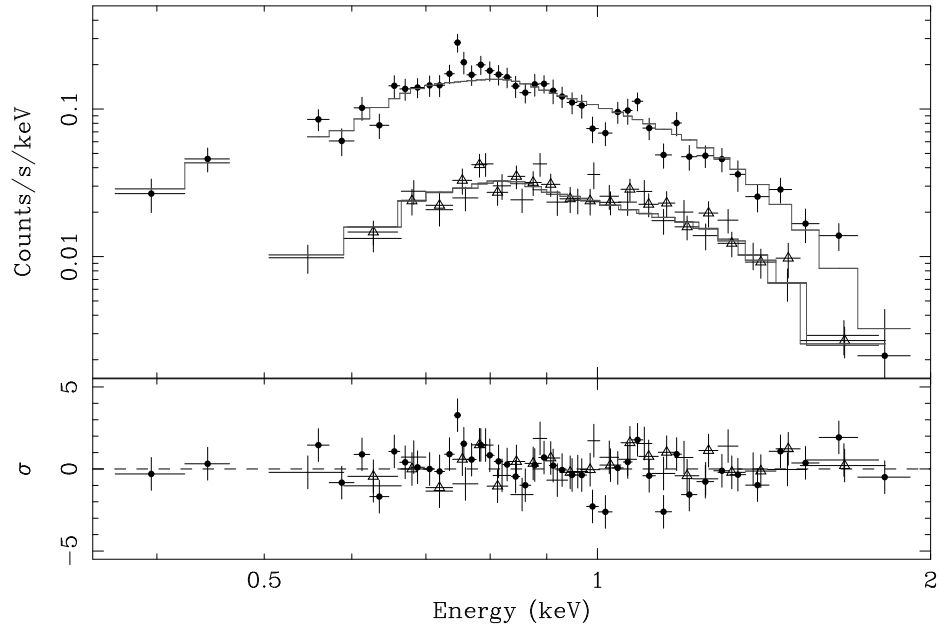


FIG. 5.— Top: *XMM-Newton* EPIC-PN (filled circles), MOS1 (black cross), and MOS2 (triangles) spectra for PSR J1819–1458, modeled as an absorbed blackbody and Gaussian line (column 2 of Table 1). Grey lines show the fitted model. The PN data have been binned with 40 counts per bin and the MOS1 and MOS2 data with 30 counts per bin to show that the best-fit model is not dependent on the spectral binning parameters. We have omitted all photons with energies from 0.5–0.53 keV as we believe that the feature in this range is due to the Oxygen edge (see Section 2.2). Bottom: residuals of the above fits.